

# Collaborative Strategy of Multifunctional Groups in Trifluoroacetamide Achieving Efficient and Stable Perovskite Solar Cells

Lidan Liu, Yong Li, Can Zheng, Zhike Liu, Ningyi Yuan, Jianning Ding, Dapeng Wang, and Shengzhong (Frank) Liu\*

The additive strategy is considered to be an effective scheme to purposefully passivate defect sites in perovskite materials. Herein, a small molecule trifluoroacetamide (TFAA) with C=O, —NH<sub>2</sub>, and F groups is incorporated into the perovskite precursor solution to alleviate the defect densities of the perovskite material from the source, so as to obtain high-quality FA<sub>0.85</sub>MA<sub>0.15</sub>PbI<sub>3</sub> perovskite absorber and its assembled photovoltaic devices. Thanks to the interactions of Lewis acid of C=O and undercoordinated Pb<sup>2+</sup>, N—H and I<sup>−</sup> via hydrogen bond, and F and FA<sup>+</sup> fragments, the nonradiative recombination sites are effectively inhibited, simultaneously promoting the nucleation and grain growth of perovskite. The analysis results demonstrate that the introduction of TFAA additive greatly enhances the crystal quality of bulk perovskite absorber, ameliorates the surface morphology of perovskite film, and improves the extraction and transfer abilities of photogenerated carriers from perovskite absorber. The perovskite solar cells (PSCs) based on TFAA agent yield a champion power conversion efficiency of 24.16%, 8.3% better than that of the control device (22.31%). More importantly, the modified perovskite film has good harsh humidity stability and the unpackaged PSCs maintain outstanding photovoltaic performance in atmospheric environment, thermal, and light conditions.

materials, innovative manufacturing processes, and cheap raw material costs.<sup>[2–5]</sup>

The large-scale and highly integrated process production is the inevitable development law of the photoelectric and photovoltaic modules. However, the key problem hindering the large-scale commercial PSCs is the intrinsic defect of perovskite materials.<sup>[6,7]</sup> A variety of defects on the surface and bulk of the perovskite absorber also degrade the stabilities of perovskite structure and corresponding photovoltaic devices. For a conventional FAMAPbI<sub>3</sub> perovskite material, the element defects contain organic cation vacancies of V<sub>FA</sub> and V<sub>MA</sub>, undercoordinated ions of Pb<sup>2+</sup> and I<sup>−</sup>, interstitial ions, and Pb–I antisite.<sup>[8–11]</sup> Through theoretical calculations, it is confirmed that these element defects with low formation energies form shallow energy levels as unintentional dopants,<sup>[12,13]</sup> which provide carrier recombination sites in the PSCs and shorten carrier diffusion length. The induced electron–hole recombination directly leads

to energy loss, which is also a main factor for the degradation of V<sub>OC</sub> in the cells.<sup>[14]</sup> The formation energy and content of the element defects are closely related to the stoichiometric ratio of precursors and the preparation method of PSCs. Moreover, shelf storage for a long duration or at a high treatment temperature can result in the loss of organic halide components and the formation of the undercoordinated Pb<sup>2+</sup> or PbI<sub>2</sub> in the perovskite absorber. In addition, the generalized defects in perovskite


## 1. Introduction

To meet the global confusion for energy shortage and environmental pollution, perovskite solar cells (PSCs) have become one of the most promising thin-film cells in the photovoltaic field. Since the advent of the PSCs, the power conversion efficiency (PCE) has soared from 3.8% to 25.7% in just dozen years,<sup>[1]</sup> which is directly related to the excellent performance of perovskite

L. Liu, Y. Li, C. Zheng, Z. Liu, D. Wang, S. (Frank) Liu  
Key Laboratory of Applied Surface and Colloid Chemistry  
Ministry of Education  
Shaanxi Key Laboratory for Advanced Energy Devices  
Shaanxi Engineering Lab for Advanced Energy Technology  
School of Materials Science and Engineering  
Shaanxi Normal University  
Xi'an 710119, China  
E-mail: liusz@snnu.edu.cn

N. Yuan, J. Ding  
School of Materials Science and Engineering Jiangsu Collaborative  
Innovation Center of Photovoltaic Science and Engineering Jiangsu  
Province Cultivation Base for State Key Laboratory of Photovoltaic Science  
and Technology  
Changzhou University  
Changzhou 213164, China

S. (Frank) Liu  
Dalian National Laboratory for Clean Energy  
iChEM  
Dalian Institute of Chemical Physics  
Chinese Academy of Sciences  
Dalian 116023, P. R. China

 The ORCID identification number(s) for the author(s) of this article can be found under <https://doi.org/10.1002/solr.202200284>.

DOI: 10.1002/solr.202200284

materials like grain boundaries and molecular clusters will also cause the collapse of perovskite lattice structure, which have an irreversible impact on the photovoltaic performance of PSC under long-term operation.<sup>[15]</sup>

The research experiences demonstrate that the surface morphology and crystallinity of perovskite films have the momentous impacts on the photovoltaic performance of PSCs.<sup>[16,17]</sup> How to prepare high-quality perovskite films has always been the goal of researchers, which plays a crucial factor in realizing high-performance PSCs. The additive incorporating into perovskite precursor solution is one of the effective methods to suppress defects from the source and control the crystallization process of thin films. So far, the additives with various functional groups are widely adopted in the perovskite-based photovoltaic devices, including ionic liquid,<sup>[18,19]</sup> Lewis acid or base,<sup>[20,21]</sup> quantum dots,<sup>[22,23]</sup> fullerene derivatives,<sup>[24,25]</sup> and inorganic metallic salts.<sup>[26,27]</sup> The previous literatures have confirmed that carbonyl groups with lone pair electrons, as Lewis bases, exhibit strong passivation ability by forming coordination bonds with under-coordinated lead ions.<sup>[28,29]</sup> In addition, it is reported that amino groups as capping ligands, especially in Pb-deficiency perovskite materials, form  $\text{NH}_3^+$  through protonation transfer to passivate the surface defect sites of perovskite film.<sup>[30]</sup> Furthermore, it is also noted that due to its ultrastrong electronegativity, fluorine atoms have compact interaction with lead and  $\text{MA}^+/\text{FA}^+$  cations in the form of hydrogen bonds.<sup>[31]</sup> Therefore, the fluorine-containing additives are widely applied to reduce defect density in the perovskite absorber. In addition, the fluorine with super-hydrophobicity can synergistically improve humidity stability of the devices. Based on the above discussion, our research group has also done a series of studies on the application of various functional additives in the PSCs.<sup>[15,32]</sup> Moreover, we have investigated and compared some studies on the application of functional additives in FAMAPbI<sub>3</sub> PSCs in recent years (Table S1, Supporting Information). It is found that the additives containing multifunctional groups are the best partners to achieve high-performance photovoltaic modules.

In this study, a small molecule of trifluoroacetamide (TFAA) with multifunctional groups is incorporated into the perovskite precursor solution to produce highly efficient  $\text{FA}_{0.85}\text{MA}_{0.15}\text{PbI}_3$ -based PSCs. The presence of TFAA can promote the nucleation of  $\text{PbI}_2$ , enlarge the grain size of the film, enhance the crystallinity, and control the morphology of perovskite absorber. The carbonyl group and amino unit in the TFAA molecule interact with undercoordinated lead ions to form coordination bonds, passivating nonradiative recombination sites and enhancing the extraction and transfer abilities of photogenerated carriers. Consequently, the PSCs with the TFAA additive deliver the best efficiency of 24.16%, better than the control device (22.31%). The hydrophobic trifluoride terminals of the molecule along with high-quality perovskite absorber enhance the harsh humidity stability of the film and the atmospheric environment stability of the devices.

## 2. Results and Discussion

The TFAA molecule with multifunctional units is commonly adopted as the intermediate in the field of pharmaceutical and

pesticide, and its molecular structure is presented in the inset of Figure 1a. To completely guarantee the interaction between each functional unit and targeting sites of perovskite, the TFAA agent is added into perovskite precursor solution. To systematically reveal the function of TFAA in the perovskite materials and perovskite film-forming process, serialized liquid-state NMR evaluations in solution are carried out. The  $^1\text{H}$  NMR spectra of mixture raw materials of MAI, FAI, and  $\text{PbI}_2$  in deuterated DMSO solvent are monitored, exhibiting obvious three resonance signals in the range of 8–9 ppm (Figure 1a,b), which is assigned to the protons binding with nitrogen atoms in cationic  $\text{FA}^+/\text{MA}^+$  of perovskite.<sup>[33]</sup> After introducing TFAA additive into the perovskite solution, the intensity of these resonance peaks decreases significantly and two additional new peaks seem to be split, which is due to the strong interaction between  $\text{FA}^+/\text{MA}^+$  protons and TFAA additive. The peak splitting phenomenon is also reported by the previous literature, which is originated from the generation of hydrogen bonds complexes of the amidinium moiety.<sup>[34,35]</sup> However, when the cations of  $\text{FA}^+$  and  $\text{MA}^+$  coexist in perovskite, which A-site cation plays the dominant role with the TFAA additives? As the ratio of FA/MA of A-site cation in this perovskite is 0.85:0.15, the peak splitting phenomenon is likely to come from the interaction between FA protons and TFAA. To confirm the suspect, the additional  $^1\text{H}$  NMR measurements of only FAI with TFAA additive are analyzed (Figure 1c,d). The intensity attenuation and position shift of FA resonance signal peaks are consistent with those observed in the mixture solution of perovskite and TFAA, suggesting that the proton bonds are formed between TFAA and  $\text{FA}^+$ . On the basis of the NMR spectrum of TFAA, two new peaks are integrated into two protons, respectively, and are attributed to two symmetrical amidine protons. Moreover, we also analyze the interaction effect between MAI and TFAA. The NMR spectra indicate that the peak position and intensity of TFAA additive have almost no change even if the incorporation of MAI (Figure 1e), implying that there is almost no proton correlation between  $\text{MA}^+$  and TFAA. Through the above analysis of proton resonance signals, the amide group in TFAA additive only has strong proton-binding ability with FA fragments within the perovskite. Subsequently, the correlation between fluorine in TFAA and FAI is explored (Figure 1f). The results demonstrate that the fluorine peak in TFAA shifts with intensity reduction under the condition of blending with FAI in solution, further confirming the interaction of F with FAI. The proton-binding and fluorine bonds between TFAA additives and FA fragments in perovskite precursor solution may promote the nucleation and crystallization of perovskite and be beneficial to the stability of perovskite absorber and the performance of the photovoltaic devices.

To further reveal the synergy between the functional groups in TFAA and perovskite, Fourier-transform infrared (FTIR) spectroscopy is carried out. For the pure TFAA, the obvious  $\text{C}=\text{O}$  and  $\text{N}-\text{H}$  stretching vibration peaks are detected at 1712 and  $3364\text{ cm}^{-1}$  (Figure 2a), respectively. When the TFAA additives are blended with  $\text{PbI}_2$  in the mixed DMF/DMSO solution, the  $\text{N}-\text{H}$  stretching vibration peak changes to a wide band, and even the vibration peak almost disappears, which is due to the hydrogen bonding between  $\text{N}-\text{H}$  unit and iodine. In addition, the stretching vibration peak of  $\text{C}=\text{O}$  weakens and shifts to  $1739\text{ cm}^{-1}$  (Figure 2b), suggesting that the interaction of

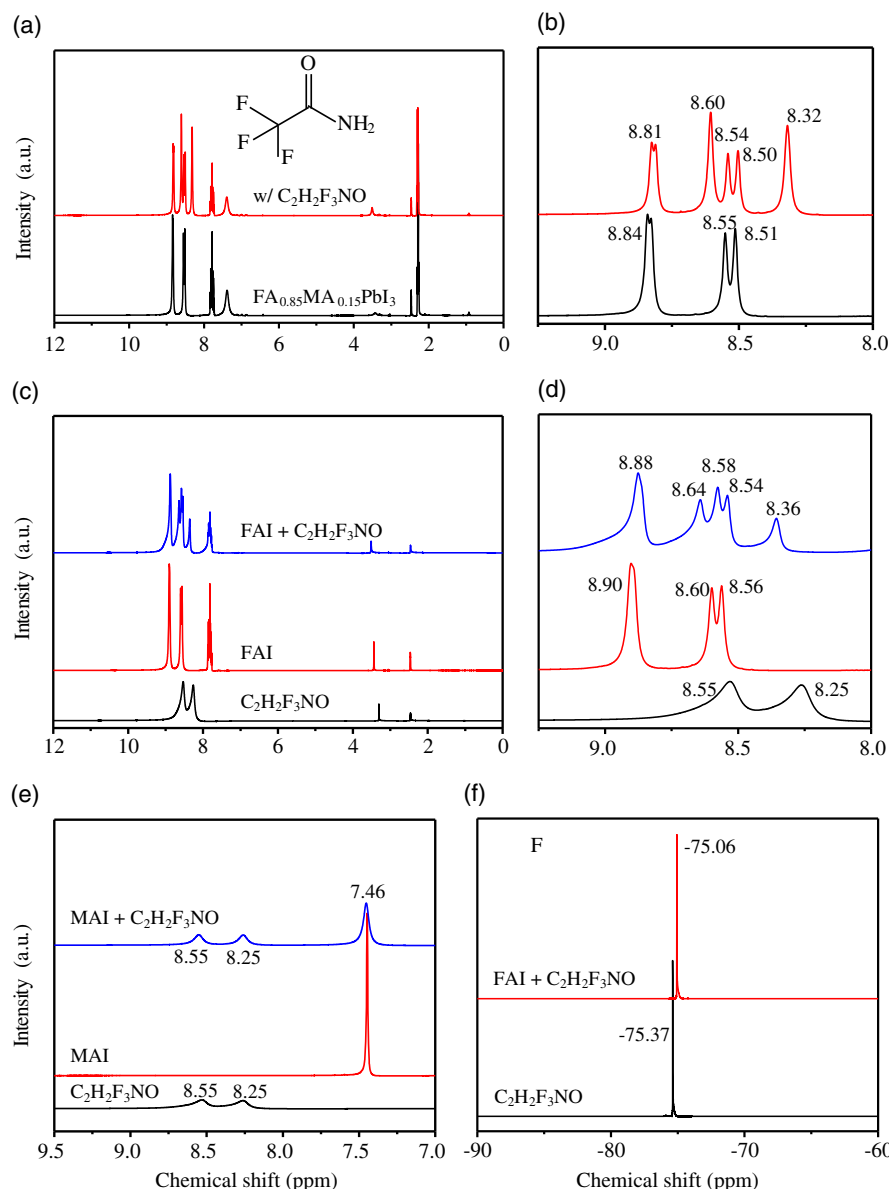


**Figure 1.** a)  $^1\text{H}$  NMR spectra and b) magnified spectra in the region of 8.0 – 9.2 ppm of  $\text{FA}_{0.85}\text{MA}_{0.15}\text{PbI}_3$  without and with TFAA additive, with the inset showing the TFAA molecule. Comparison of the c)  $^1\text{H}$  NMR spectra and d) magnified spectra in the region of 8.0 – 9.2 ppm of pure TFAA, FAI, and FAI with TFAA. e) Comparison of the  $^1\text{H}$  NMR spectra of pure TFAA, MAI, and MAI with TFAA. f)  $^{19}\text{F}$  NMR spectra of pure TFAA and FAI with TFAA.

$\text{C}=\text{O}\cdots\text{Pb}$  forms and leads to the reduction of the concentration of undercoordinated  $\text{Pb}^{2+}$  cations.<sup>[36]</sup> The previous literature has reported that in the case of good configuration of  $\text{N}-\text{H}$  and  $\text{C}=\text{O}$ , the hydrogen bond between  $\text{N}-\text{H}$  unit and  $\text{I}$  assists in passivating the antisite  $\text{Pb}$  defects,<sup>[37]</sup> so as to maximize the benefits of passivation efficacy of various functional groups. X-ray photoelectron spectroscopy (XPS) are measured to explore the elemental composition and chemical bond states on the surface of perovskite samples. Figure 2c exhibits the full range spectra of perovskite samples without and with TFAA modification, clearly stating that the incorporation of TFAA agents hardly changes the elementary composition and corresponding peak intensity. Unfortunately, the signal of  $\text{F}$  is barely detected, possibly because

the amount of introduced additives is trace and cannot meet the detection accuracy of the equipment. When the  $\text{Pb}$  4f region is finely amplified (Figure 2d), two peaks at 137.66 and 142.53 eV in the pristine sample are originated from the excited electrons of the 4f 7/2 and 4f 5/2 orbitals of  $\text{Pb}^{2+}$ ,<sup>[38]</sup> respectively. For the TFAA-modified sample, both peaks shift 0.15 eV along the low binding energy direction, which may be due to the strong electronic interaction between the  $\text{C}=\text{O}$  unit of TFAA and  $\text{Pb}^{2+}$ . The electron cloud transfer of carbonyl group has a shielding effect on the  $\text{Pb}$  nucleus, resulting in the reduction of the binding energy of electrons in the inner layer of  $\text{Pb}$  atom.<sup>[34,39]</sup> After the TFAA treatment, the identical phenomenon also occurs on  $\text{I}$  3d and  $\text{N}$  1s peaks (Figure 2e,f), indicating that the TFAA

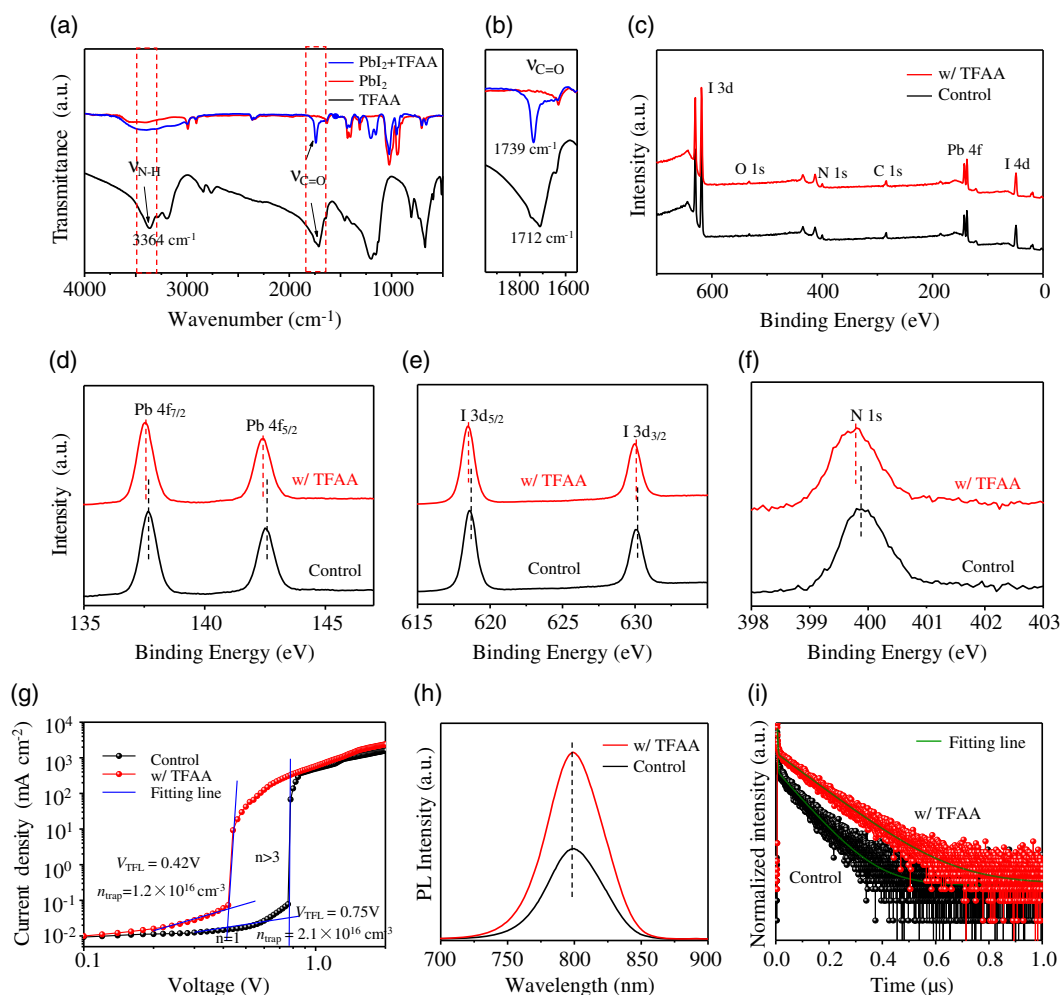


**Figure 2.** a) FTIR spectra and b) magnified spectra in the region of  $1550 - 1950 \text{ cm}^{-1}$  of pure TFAA,  $\text{PbI}_2$ , and  $\text{PbI}_2$  with TFAA. c) The whole XPS spectra and the spectra of d) Pb 4f, e) I 3d, and f) N 1s of perovskite films without and with TFAA modification. g) The  $I - V$  curves of the electron-dominated devices with the structure of FTO/ $\text{TiO}_2$ /perovskite without and with TFAA/PCBM/Ag. h) Steady-state PL and i) TRPL spectra of perovskite films without and with TFAA additive.

additives form the bonds with each component of perovskite, which is consistent with NMR and FTIR results. Therefore, the chemical bond state analysis demonstrates that each functional group of TFAA additive has an electrostatic interaction with perovskite defect sites, thereby contributing the enhanced crystallinity accompanied with oriented growth, which provides a sufficient prerequisite for stable perovskite films and their photovoltaic devices.

To quantitatively explore the passivation behavior of TFAA additives on the overall defect densities of states of perovskite, the electron-dominated devices with the architecture of FTO/ $\text{TiO}_2$ /perovskite without and with TFAA/PCBM/Ag are prepared and characterized under various bias voltages in the dark (Figure 2g). In the current–voltage ( $I - V$ ) curves, a kink point voltage between the ohmic and trap-filled regions is generally named as trap-filling limit voltage ( $V_{\text{TFL}}$ ). The  $V_{\text{TFL}}$  values of the devices before and after TFAA modification are 0.75 and 0.42 V, respectively. According to the functional relationship between trap-state density and  $V_{\text{TFL}}$ ,<sup>[40,41]</sup> the trap densities of

the device with TFAA treatment is  $1.2 \times 10^{16} \text{ cm}^{-3}$ , about half lower than that of the control device ( $2.1 \times 10^{16} \text{ cm}^{-3}$ ). Meanwhile, the passivation effect of TFAA additive on hole-based devices with the structure of FTO/PEDOT:PSS/perovskite without and with TFAA/Spiro-OMeTAD/Au was evaluated (Figure S1, Supporting Information). The corresponding  $V_{\text{TFL}}$  values are 0.68 and 0.47 V, and the calculated trap densities are  $1.9$  and  $1.3 \times 10^{16} \text{ cm}^{-3}$ , respectively. Apparently, the TFAA-treated perovskite exhibits the high crystal quality as well as reduced electron and hole trap densities. The above conclusions can be cross-checked by the change of photoluminescence (PL) intensity because the PL behavior of perovskite films can reflect the charge carrier dynamics and is directly influenced by the trap density. Figure 2h presents the steady-state PL spectra of glass/perovskite before and after TFAA additives. In contrast, although the PL peak position remains unchanged at 799 nm, the PL intensity of TFAA-modified perovskite sample is over 2 times higher than that of the pristine film, indicating that the TFAA additive notably passivates nonradiative



recombination caused by charge carrier trap centers. Subsequently, based on the same samples, the time-resolved PL (TRPL) attenuation measurements (Figure 2i) indicate that the average charge lifetime ( $\tau_{\text{ave}}$ ) increases significantly from 93.2 ns for the pristine perovskite to 142.7 ns for the TFAA-modified sample (Table S2, Supporting Information), further confirming that the additive weakens defect-assisted nonradiative recombination, which is also helped to explore the origin of the increase in open-circuit voltage ( $V_{\text{OC}}$ ).<sup>[42]</sup>

According to the abovementioned interaction mechanism between functional groups in TFAA and perovskite defect sites, the influence of TFAA on the micromorphology and appearance of perovskite is comprehensively evaluated. **Figure 3a** shows the surface morphology of perovskite films with different concentrations of TFAA, and the corresponding grain size distributions are plotted in the inset. All samples exhibit good surface coverage without pinhole. Apparently, the average grain size of the TFAA-treated samples enlarges significantly, which increases from 243 nm for the control sample to 440 nm for 1 mg mL<sup>-1</sup> TFAA-modified film and continuously grows to 595 nm for 5 mg mL<sup>-1</sup> TFAA-treated sample, and then decreases slightly with the increase in the TFAA concentration. The perovskite absorber with grain growth of nearly 2.5 times is rooted in the generation of a PbI<sub>2</sub>-TFAA adduct, which raises the activation energy and reduces the number of nucleation, delaying the crystallization process and enlarging the grain size. Thus, the decrease in the grain boundary and surface defects is positively correlated with the performance of the PSCs. However, the

excess TFAA concentration interferes with the perovskite crystallization process, in turn leading to the reduction in the grain size.

Accordingly, the atomic force microscopy (AFM) topography images (Figure 3b) further indicate that the incorporation of TFAA additives has greatly smoothed the root-mean-square surface roughness that gradient decreases from 27.1 nm for the control sample to 15.1 nm for 5 mg mL<sup>-1</sup> TFAA-modified film, and then slightly increases with the continuous increase of TFAA concentration. In addition, the energy-dispersive spectrometry (EDS) element mapping of the pristine and 5 mg mL<sup>-1</sup> TFAA-modified perovskite samples is performed (Figure S2, Supporting Information). The elements in all samples are evenly distributed on the surface of perovskite films, and the good dispersion of F element also proves that the TFAA additive exists in the perovskite absorber. The atomic ratio of I/Pb increases from 2.65 in the control sample to 2.87 in the TFAA-modified perovskite film, and the proportion of I element in the treated film increases. These results suggest that TFAA additive can prevent the precipitation of iodine in the precursor solution during the film-forming process and ensure that the atomic ratio of the perovskite is close to the ideal stoichiometric ratio of FA<sub>0.85</sub>MA<sub>0.15</sub>PbI<sub>3</sub>. The change monitoring of TFAA additives on the crystallinity of perovskite films is then executed by X-ray diffraction (XRD) measurement (Figure S3, Supporting Information). The perovskite samples modified with different concentrations of TFAA additives have diffraction peaks with the same peak position as the control sample, including the (110) plane of perovskite at 13.92° and the hexagonal PbI<sub>2</sub> peak

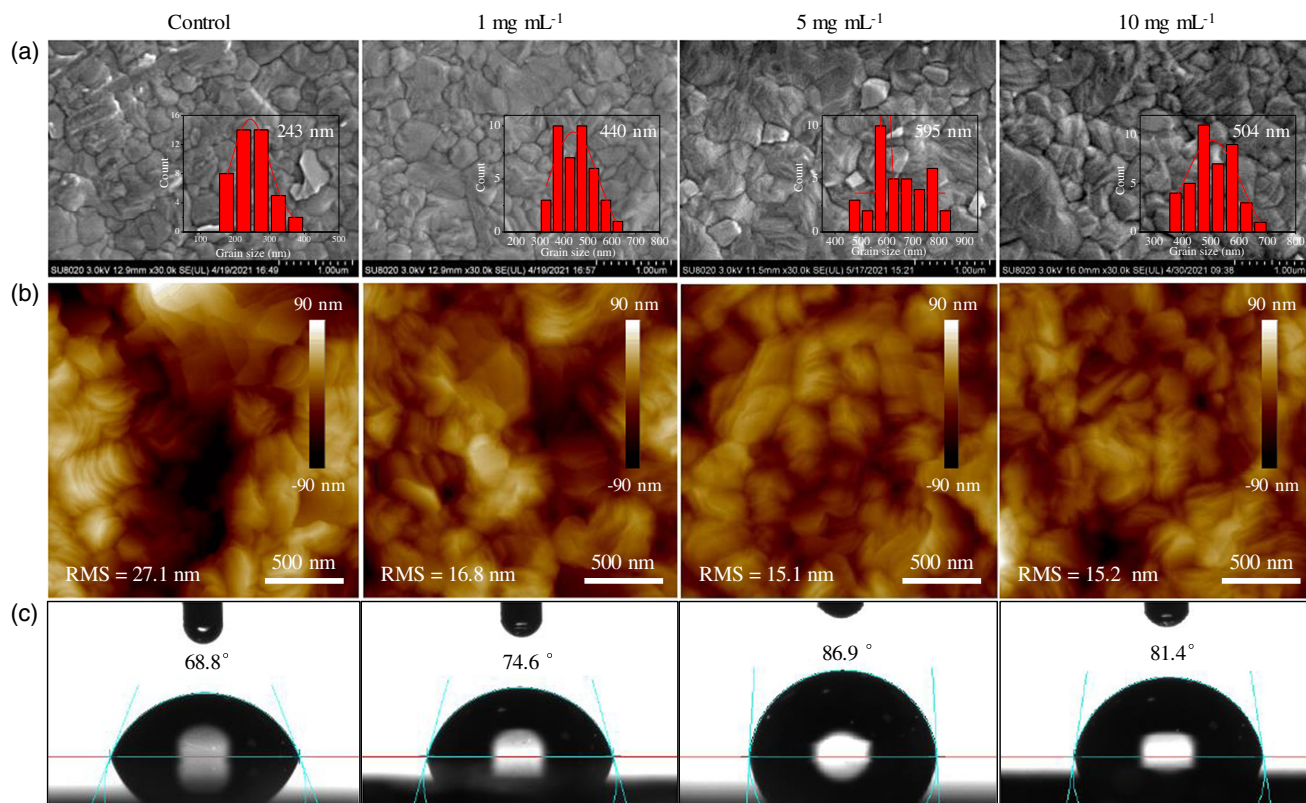


**Figure 3.** a) Top-view SEM images, b) AFM images, and c) the water contact angles of perovskite films modified with different concentrations of TFAA additive, with the corresponding grain size distribution in the insets of SEM images.

at 12.64°, suggesting that TFAA additives have no effect on the lattice parameters of perovskite. However, with the increase in TFAA concentration, the intensity of (110) plane of perovskite gradually rises, and the peak proportion of perovskite to PbI<sub>2</sub> gradually increases. It is confirmed that the TFAA additives can improve the crystal nucleation process of perovskite, which is consistent with the grain enlargement in SEM measurement. Then, the water contact angle test is conducted to track the hydrophobicity of TFAA on the perovskite surface (Figure 3c). Compared with the pristine sample, the contact angle of the film containing the TFAA becomes larger and enlarges with the increase of TFAA content, and reaches the maximum value of 86.9° when the TFAA concentration is 5 mg mL<sup>-1</sup>. Further increasing the TFAA concentration to 10 mg mL<sup>-1</sup> slightly reduces the contact angle. Based on Wenzel theory, for water contact angle less than 90°, the hydrophobicity mainly depends on the surface roughness of the film.<sup>[43,44]</sup> In addition, because of the hydrophobic characteristics of the F terminals in the TFAA molecule, the surface energy of the treated perovskite film decreases. Due to the moisture-proof shielding effect of TFAA, the degradation probability of perovskite films in air is reduced, which eventually contributes to the environmental stability of the PSCs.

Ultraviolet photoelectron spectroscopy (UPS) is adopted to evaluate the energy levels of perovskite films before and after TFAA modification. The energy levels of the pristine and resulting perovskite are calculated by the cutoff and onset positions in the UPS spectra (Figure S4, Supporting Information). According to the functional relationships of the Fermi level  $E_F = h\nu - E_{\text{cutoff}}$  and the valence band maximum  $E_V = 21.22 - (E_{\text{cutoff}} - E_{\text{onset}})$ ,<sup>[45,46]</sup> the  $E_F$  and  $E_V$  values shift from -4.30 and -5.62 eV for the control sample to -4.26 and -5.53 eV for TFAA-treated perovskite film, respectively. Combined with the almost constant optical bandgap value of 1.55 eV (Figure S5, Supporting Information), the conduction band minimum  $E_C$  values of perovskite without and with treatment are located at -4.07 and -3.98 eV, respectively. The energy band arrangement of perovskite in the PSCs can be naturally depicted (Figure 4a). Figure S6, Supporting Information, shows the cross-sectional SEM images of the PSCs without and with TFAA modification, and the thickness of all perovskite absorbers is ≈500 nm. The upward movement of the  $E_F$  and  $E_V$  provides an internal driving force for the extraction and transfer of photogenerated holes, which is mainly because of the electron donor and passivation effect of carbonyl groups and fluorine terminals in TFAA. The lone pair electrons on the carbonyl groups move from the TFAA to Pb<sup>2+</sup> cations, contributing to the raise in the Fermi level and inactivate the defect energy level in the perovskite, which is conducive to improving the  $V_{OC}$  and photovoltaic performance of the devices. Figure 4b exhibits the photocurrent density versus voltage ( $J$ - $V$ ) plots for the champion cells after the optimization of various TFAA concentrations with the extracted photovoltaic parameters tabulated in the inset. The control device delivers a best PCE of 22.31%, with a  $V_{OC}$  of 1.117 V, a short-circuit current ( $J_{SC}$ ) of 25.01 mA cm<sup>-2</sup>, and a fill factor (FF) of 79.81%. Comparatively, for the devices modified by the TFAA, the PCEs of the corresponding PSCs increase with the increasing of the additive concentration, and then slightly decrease when the TFAA concentration further increases. The champion PCE of

24.16% is obtained for device with the TFAA concentration of 5 mg mL<sup>-1</sup>, accompanied by the  $V_{OC}$  of 1.157 V,  $J_{SC}$  of 25.59 mA cm<sup>-2</sup>, and FF of 81.63%. The credibility of the  $J_{SC}$  is confirmed by the external quantum efficiency (EQE) spectra (Figure 4c). The integrated  $J_{SC}$  for the control and TFAA-modified devices are 24.88 and 25.23 mA cm<sup>-2</sup>, respectively, which are in conformity with the  $J_{SC}$  values extracted from the  $J$ - $V$  curves (<1.5% discrepancy). The significant enhancement of  $V_{OC}$  and FF mainly originates from the high-quality perovskite absorber and comprehensive passivation effect of the TFAA additives. It is known that the notorious hysteresis is caused by the imbalance of carrier extraction in the perovskite and transfer in the adjacent transfer layers. Figure 4d presents the  $J$ - $V$  curves of the PSCs without and with TFAA additive in both the reverse and forward scan, and the corresponding hysteresis index ( $HI = (PCE_{\text{reverse}} - PCE_{\text{forward}})/PCE_{\text{reverse}}$ ) are listed in Table S3, Supporting Information.<sup>[47,48]</sup> The calculated HI remarkably reduces from 14.12% for the control device to 2.32% for the TFAA-modified cell, suggesting that the incorporation of the TFAA greatly passivates the defect density in the perovskite and facilitates the charge extraction from the perovskite/Spiro-OMeTAD interface. To explore the reproducibility of device performance, the statistical distribution of photovoltaic parameters of 40 cells is depicted (Figure S7, Supporting Information) and the average photovoltaic parameters with standard deviation are tabulated (Table S4, Supporting Information). The PSCs with 5 mg mL<sup>-1</sup> TFAA additive present the outstanding performance with narrow photovoltaic parameter distribution, further confirming that the introduction of TFAA does contribute to high-performance devices. In addition, the stabilized maximum power point (MPP) for the PSCs is tracked for 600 s under 1 sun illumination (Figure 4e). The photocurrent of the control and TFAA-modified devices stabilize at 24.86 and 25.21 mA cm<sup>-2</sup> at their MPP voltages, yielding to the PCEs of 21.88% and 23.70%, respectively. The stable output results demonstrate that TFAA assists in improving the device stability under continuous illumination.

To clarify the inner carrier transfer and recombination process of the devices, the electrochemical impedance spectroscopy (EIS) measurements are conducted at a bias voltage of 0.98 V. Figure 4f describes the Nyquist plots of the PSCs before and after TFAA modification with the equivalent circuit (Figure S8, Supporting Information). The related impedance parameters are tabulated in Table S5, Supporting Information. Apparently, the TFAA-modified device has the smaller series resistance  $R_s$  and transfer resistance  $R_{tr}$ , and the larger recombination resistance  $R_{rec}$  compared with those of the control device, which reflects the fast charge transfer and low carrier recombination probability of TFAA-based PSCs, in agreement with the enhanced FF. In addition, the dark current density of the TFAA-modified device almost reduces by two orders of magnitude than the control cell (Figure 4g), confirming that the modified device exhibits less defect and more photocurrent flows through the device, which is stemmed from the formation of high-quality perovskite absorber and efficient charge carrier transfer.<sup>[49]</sup> Mott-Schottky curves are plotted to comprehend the internal electric field distribution of device using the built-in potential ( $V_{bi}$ ) by extrapolating the curve of  $1/C^2$ - $V$  to zero (Figure 4h). In contrast to the control device, the TFAA-modified PSC has the reduced

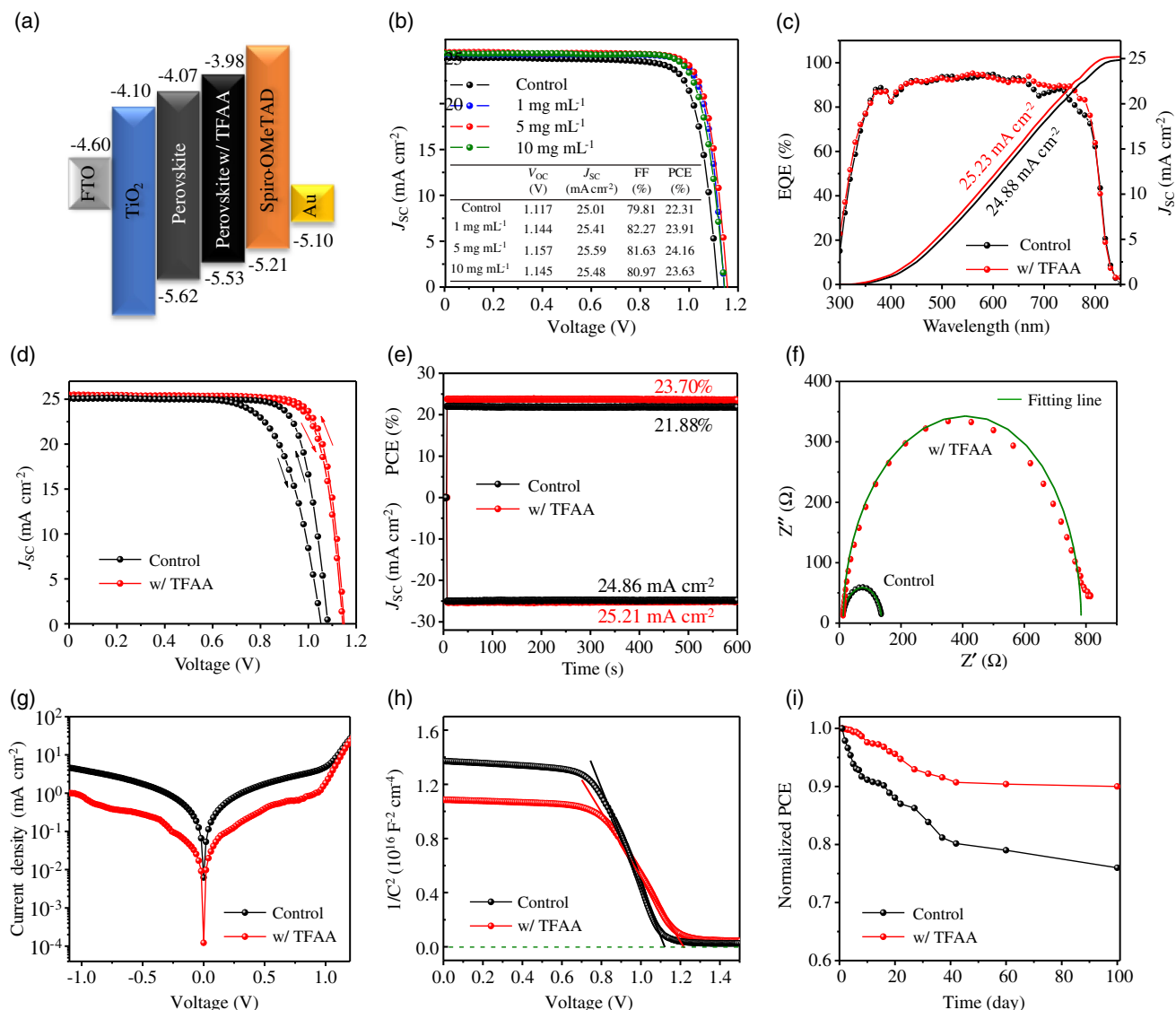


**Figure 4.** a) Energy-level diagram and b)  $J$ - $V$  curves with champion photovoltaic parameters in the inset, c) EQE spectra, d)  $J$ - $V$  curves scanned in different directions, e) stable output, f) Nyquist plots with the equivalent circuit model in the inset, g) dark  $J$ - $V$  curves, h) Mott-Schottky plots, and i) the ambient storage stability of the PSCs without and with TFAA additive.

capacitance and enhanced  $V_{bi}$  with steep slope, demonstrating that the small charge accumulation at the adjacent interfaces. The high  $V_{bi}$  implies large capacity to separate the carriers, which is originated from the favorable band structure, thereby contributing to the high  $V_{OC}$  of modified device.<sup>[39,46]</sup> To deeply analyze the charge transport process and carrier recombination dynamics, the light-intensity-dependent  $J$ - $V$  test on the devices without and with TFAA modification is carried out (Figure S9, Supporting Information). In the semilogarithmic scale, the TFAA-modified device has a slope of  $1.51 K_B T q^{-1}$ , which is much lower than that of the control PSC ( $2.18 K_B T q^{-1}$ ). In terms of the dependence of  $V_{OC}$  on light intensity, the unit slope deviating from 1 embodies the recombination probability. Therefore, trap-assisted recombination in the perovskite absorber has been successfully suppressed and the TFAA-based device shows a low-

level Shockley-Read-Hall recombination.<sup>[50]</sup> Concurrently, the dependence of  $J_{SC}$  on light intensity is evaluated on the basis of the power-law of  $J_{SC} = I^\alpha$ , where the exponent  $\alpha$  stands for the degree of freedom of space charge limit.<sup>[50]</sup> For the control and TFAA-based devices, the  $\alpha$  values are 0.957 and 0.961, respectively (Figure S10, Supporting Information). The TFAA-modified PSC with large  $\alpha$  exhibits negligible space limited charge characteristics, decreasing bimolecular charge carrier recombination. Subsequently, the carrier recombination probability in the cells is explored by the  $V_{OC}$  decay measurements (Figure S11, Supporting Information). The photovoltage decay lifetime is extended from 0.91 ms for the control device to 1.15 ms after TFAA modification, suggesting that interfacial recombination has been suppressed. On the basis of the above results, TFAA has obvious passivation effect on perovskite, which

is of great help to the improvement of cell performance. In addition to considering considerable efficiency, another important index of the PSCs is the long-term stability. To explore the operational stability of devices without and with the TFAA additives, the unencapsulated cells are stored in air at a temperature of 25 °C with a relative humidity of  $\approx 30\%$  (Figure 4i). After 100 days of storage, the efficiency of the TFAA-modified PSCs first decays and then stabilizes with the storage duration, and finally lost only 9% of the initial PCE, while the photovoltaic performance of the control cell deteriorates by  $>20\%$  and maintains a continuous deterioration trend. The improvement of device stability is mainly due to the auxiliary improvement of crystallinity of perovskite absorber, passivation of surface and grain boundary defects, and enhancement of hydrophobicity on the perovskite surface by TFAA additives.

To further explore the humidity stability, the perovskite films are directly exposed to harsh ambient air with a relative humidity of 85%. Figure 5a exhibits the photographs of the surface

morphology evolution of perovskite films without and with TFAA additives. When the control sample is stored for 8 h, the film color gradually fades from black and turns white at the edge. After aging for 16 h, the discolored edge gradually expands to almost half of the sample, meaning that the water erosion is carried out by vulnerable sites. In contrast, the perovskite film modified with TFAA remains black even after 16 h. Simultaneously, XRD measurement is adopted to visually track the crystallization and phase transfer process of perovskite film. For the as-fabricated film (Figure 5b), although a weak  $\text{PbI}_2$  diffraction peak can be obtained at  $12.86^\circ$ , the perovskite (110) crystal plane still appears as the main diffraction peak at  $14.08^\circ$ . After aging 4 h, additional  $\delta$ -phase perovskite peak appears at  $11.96^\circ$ . As time goes on, the peak intensity of  $\alpha$ -phase perovskite gradient decreases, while the intensities of  $\delta$ -phase perovskite peak and  $\text{PbI}_2$  phase diffraction peak gradually enhances. When the control sample was subjected to humidity attack for 16 h, the obvious perovskite phase transfer from  $\alpha$ -phase to  $\delta$ -phase

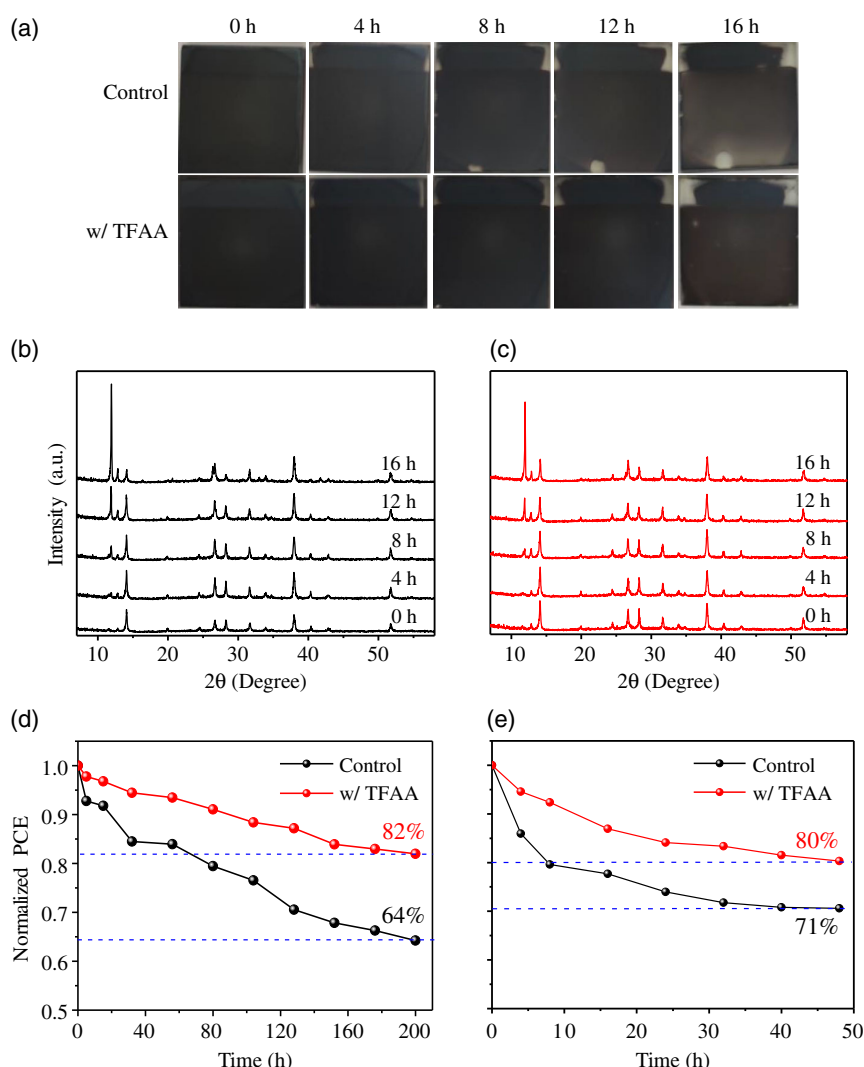


**Figure 5.** a) Photographs of perovskite films without and with TFAA additive aged in ambient air with 85% relative humidity conditions; variation in XRD patterns of corresponding b) control and c) TFAA-modified perovskite films as a function of the duration under the harsh-humidity environment. d) The thermal and e) light stabilities of the devices without and with TFAA additive.



occurs, and the intensity of  $\alpha$ -phase perovskite decays to be weaker than that of  $\text{PbI}_2$  phase. According to the TFAA-modified perovskite (Figure 5c), the as-formed film has a relatively high intensity of  $\alpha$ -phase perovskite peak. During the 8 h humidity aging stage, the  $\delta$ -phase perovskite is detected. Although the  $\delta$ -phase perovskite increases after storage for 16 h, its intensity is much lower than that of the control film. The intensity of  $\alpha$ -phase perovskite is always dominant compared with that of  $\text{PbI}_2$  phase, which may be attributed to the moisture-proof shielding effect of the TFAA additives. In addition, the thermal stability of the unsealed device before and after TFAA modification is also evaluated in  $\text{N}_2$  atmosphere at 85 °C (Figure 5d). According to the trend of normalized efficiency, within the duration of 200 h, the efficiency of the control device decreases rapidly to  $\approx 64\%$  of the initial value, while the PSC containing TFAA decreases tenderly and maintains  $\approx 82\%$  of the beginning PCE. Simultaneously, to monitor the light stability of the cell under sunlight, the simulated AM1.5G illumination is adopted to evaluate the photovoltaic characteristics of the unsealed device (Figure 5e). Under the light illumination for 48 h, the PCE of untreated cell deteriorates rapidly by 30%, while the TFAA-passivated PSC keeps  $>80\%$  of its initial efficiency at the identical duration. In brief, the results of thermal stability and photostability intuitively demonstrate that using TFAA as a multifunctional additive is a promising strategy to improve the stability of the most advanced PSCs.

### 3. Conclusions

In summary, we have incorporated a small TFAA molecule with  $\text{C}=\text{O}$ ,  $-\text{NH}_2$ , and F groups into perovskite precursor solution to promote the nucleation and grain growth of perovskite from the source. Due to the interactions of Lewis acid of  $\text{C}=\text{O}$  and under-coordinated  $\text{Pb}^{2+}$ ,  $\text{N}-\text{H}$ , and  $\text{I}^-$  via hydrogen bond, and F and  $\text{FA}^+$  fragments, the nonradiative recombination sites are effectively passivated and the defect density of perovskite materials is remarkably reduced. The high crystal quality, smooth film surface morphology, and suitable energy-level matching arrangement of perovskite absorber are more conducive to the extraction and transfer of photogenerated carriers. On the basis of the comprehensive function of TFAA additive, the efficiency is increased by 8.3% from 22.31% for the control cell to 24.16% for the modified device. In parallel, according to the moisture-proof shielding effect of hydrophobic trifluoride terminals in the TFAA additive, the modified perovskite film presents good harsh humidity stability, and corresponding unpackaged PSCs hold outstanding atmospheric environment, thermal, and light stabilities.

### Supporting Information

Supporting Information is available from the Wiley Online Library or from the author.

### Acknowledgements

L.L. and Y.L. contributed equally to this work. The authors acknowledge support from the National Nature Science Foundation of China (grant no. 62174103), the Natural Science Basic Research Plan in Shaanxi

Province of China (grant nos. 2020NY-159 and 2020JM-297), the Fundamental Research Funds for the Central Universities (grant no. GK202103052), the Changjiang Scholar and the Innovative Research Team (grant no. IRT\_14R33), the 111 Project (grant no. B21005), and the Chinese National 1000-talent-plan program (grant no. 111001034).

### Conflict of Interest

The authors declare no conflict of interest.

### Data Availability Statement

Research data are not shared

### Keywords

collaborative strategy, multifunctional groups, perovskites, solar cells, trifluoroacetamide

Received: March 29, 2022

Revised: May 5, 2022

Published online:

- [1] A. Kojima, K. Teshima, Y. Shirai, T. Miyasaka, *J. Am. Chem. Soc.* **2009**, 131, 6050.
- [2] J. W. Lee, H. Yu, K. Lee, S. Bae, J. Kim, G. R. Han, D. Hwang, S. K. Kim, J. Jang, *J. Am. Chem. Soc.* **2019**, 141, 5808.
- [3] Z. Liu, J. Hu, H. Jiao, L. Li, G. Zheng, Y. Chen, Y. Huang, Q. Zhang, C. Shen, Q. Chen, H. Zhou, *Adv. Mater.* **2017**, 29, 1606774.
- [4] S. D. Stranks, G. E. Eperon, G. Grancini, C. Menelaou, M. J. Alcocer, T. Leijtens, L. M. Herz, A. Petrozza, H. J. Snaith, *Science* **2013**, 342, 341.
- [5] Y. Liu, Z. Yang, D. Cui, X. Ren, J. Sun, X. Liu, J. Zhang, Q. Wei, H. Fan, F. Yu, X. Zhang, C. Zhao, S. F. Liu, *Adv. Mater.* **2015**, 27, 5176.
- [6] D. Liu, D. Luo, A. N. Iqbal, K. W. P. Orr, T. A. S. Doherty, Z. H. Lu, S. D. Stranks, W. Zhang, *Nat. Mater.* **2021**, 20, 1337.
- [7] B. Gao, J. Hu, S. Tang, X. Xiao, H. Chen, Z. Zuo, Q. Qi, Z. Peng, J. Wen, D. Zou, *Adv. Sci.* **2021**, 8, e2102081.
- [8] D. J. Keeble, J. Wiktor, S. K. Pathak, L. J. Phillips, M. Dickmann, K. Durose, H. J. Snaith, W. Egger, *Nat. Commun.* **2021**, 12, 5566.
- [9] J. S. Yun, J. Seidel, J. Kim, A. M. Soufiani, S. Huang, J. Lau, N. J. Jeon, S. I. Seok, M. A. Green, A. Ho-Baillie, *Adv. Energy Mater.* **2016**, 6, 1600330.
- [10] X. Liu, Z. Yu, T. Wang, K. L. Chiu, F. Lin, H. Gong, L. Ding, Y. Cheng, *Adv. Energy Mater.* **2020**, 10, 2001958.
- [11] H. Si, C. Xu, Y. Ou, G. Zhang, W. Fan, Z. Xiong, A. Kausar, Q. Liao, Z. Zhang, A. Sattar, Z. Kang, Y. Zhang, *Nano Energy* **2020**, 68, 104320.
- [12] C. Eames, J. M. Frost, P. R. Barnes, B. C. O'Regan, A. Walsh, M. S. Islam, *Nat. Commun.* **2015**, 6, 7497.
- [13] J. Kim, S. H. Lee, J. H. Lee, K. H. Hong, *J. Phys. Chem. Lett.* **2014**, 5, 1312.
- [14] Y. Guo, J. Ma, H. Lei, F. Yao, B. Li, L. Xiong, G. Fang, *J. Mater. Chem. A* **2018**, 6, 5919.
- [15] F. Qian, S. Yuan, Y. Cai, Y. Han, H. Zhao, J. Sun, Z. Liu, S. Liu, *Sol. RRL* **2019**, 3, 1900072.
- [16] H. Li, G. Wu, W. Li, Y. Zhang, Z. Liu, D. Wang, S. F. Liu, *Adv. Sci.* **2019**, 6, 1901241.
- [17] H. Li, D. Li, W. Zhao, S. Yuan, Z. Liu, D. Wang, S. Liu, *J. Power Sources* **2020**, 448, 227586.

- [18] S. Bai, P. Da, C. Li, Z. Wang, Z. Yuan, F. Fu, M. Kaweck, X. Liu, N. Sakai, J. T. Wang, S. Huettner, S. Buecheler, M. Fahlman, F. Gao, H. J. Snaith, *Nature* **2019**, 571, 245.
- [19] Y. Zhang, Z. Fei, P. Gao, Y. Lee, F. F. Tirani, R. Scopelliti, Y. Feng, P. J. Dyson, M. K. Nazeeruddin, *Adv. Mater.* **2017**, 29, 1702157.
- [20] J.-W. Lee, S.-H. Bae, Y.-T. Hsieh, N. De Marco, M. Wang, P. Sun, Y. Yang, *Chem* **2017**, 3, 290.
- [21] N. K. Noel, A. Abate, S. D. Stranks, E. S. Parrott, V. M. Burlakov, A. Goriely, H. J. Snaith, *ACS Nano* **2014**, 8, 9815.
- [22] Y. Yang, W. Wang, *J. Power Sources* **2015**, 293, 577.
- [23] J. Duan, Y. Zhao, B. He, Z. Jiao, Q. Tang, *Electrochim. Acta* **2018**, 282, 263.
- [24] Y. Shao, Z. Xiao, C. Bi, Y. Yuan, J. Huang, *Nat. Commun.* **2014**, 5, 5784.
- [25] Z. Zhu, C. C. Chueh, F. Lin, A. K. Jen, *Adv. Sci.* **2016**, 3, 1600027.
- [26] J. Zhang, Y. Fang, W. Zhao, R. Han, J. Wen, S. F. Liu, *Adv. Mater.* **2021**, 33, e2103770.
- [27] G. Yang, P. Qin, G. Fang, G. Li, *J. Energ. Chem.* **2018**, 27, 962.
- [28] Y. Cai, J. Cui, M. Chen, M. Zhang, Y. Han, F. Qian, H. Zhao, S. Yang, Z. Yang, H. Bian, T. Wang, K. Guo, M. Cai, S. Dai, Z. Liu, S. Liu, *Adv. Funct. Mater.* **2020**, 31, 2005776.
- [29] G. Wu, H. Li, J. Cui, Y. Zhang, S. Olthof, S. Chen, Z. Liu, D. Wang, S. F. Liu, *Adv. Sci.* **2020**, 7, 1903250.
- [30] B. Luo, S. B. Naghadeh, A. L. Allen, X. Li, J. Z. Zhang, *Adv. Funct. Mater.* **2017**, 27, 1604018.
- [31] C. Liu, S. Liu, Y. Wang, Y. Chu, K. Yang, X. Wang, C. Gao, Q. Wang, J. Du, S. Li, Y. Hu, Y. Rong, L. Guo, A. Mei, H. Han, *Adv. Funct. Mater.* **2021**, 31, 2010603.
- [32] S. Yuan, F. Qian, S. Yang, Y. Cai, Q. Wang, J. Sun, Z. Liu, S. Liu, *Adv. Funct. Mater.* **2019**, 29, 1807580.
- [33] T. Liu, Y. Liu, M. Chen, X. Guo, S. Tang, R. Zhang, Z. Xie, J. Wang, A. Gu, S. Lin, N. Wang, *Adv. Funct. Mater.* **2021**, 32, 2106779.
- [34] C. Qin, T. Matsushima, T. Fujihara, C. Adachi, *Adv. Mater.* **2017**, 29, 1603808.
- [35] M. Yavari, M. Mazloum-Ardakani, S. Gholipour, N. Marinova, J. L. Delgado, S. H. Turren-Cruz, K. Domanski, N. Taghavinia, M. Saliba, M. Grätzel, A. Hagfeldt, W. Tress, *Adv. Energy Mater.* **2018**, 8, 1702719.
- [36] Z. Zhang, J. Jiang, X. Xiao Liu, X. Wang, L. Wang, Y. Qiu, Z. Zhang, Y. Zheng, X. Wu, J. Liang, C. Tian, C. C. Chen, *Small* **2021**, e2105184.
- [37] R. Wang, J. Xue, K. L. Wang, Z. K. Wang, Y. Luo, D. Fenning, G. Xu, S. Nuryyeva, T. Huang, Y. Zhao, J. L. Yang, J. Zhu, M. Wang, S. Tan, I. Yavuz, K. N. Houk, Y. Yang, *Science* **2019**, 366, 1509.
- [38] X. Xu, X. Ji, R. Chen, F. Ye, S. Liu, S. Zhang, W. Chen, Y. Wu, W. H. Zhu, *Adv. Funct. Mater.* **2021**, 2109968.
- [39] H. Zhang, Z. Yan, Y. Xu, X. Wang, J. Wu, Z. Lan, *Adv. Mater. Interfaces* **2021**, 9, 2101463.
- [40] Z. Wang, Y. Lu, Z. Xu, J. Hu, Y. Chen, C. Zhang, Y. Wang, F. Guo, Y. Mai, *Adv. Sci.* **2021**, 8, e2101856.
- [41] K. Wang, W. Zhao, J. Liu, J. Niu, Y. Liu, X. Ren, J. Feng, Z. Liu, J. Sun, D. Wang, S. F. Liu, *ACS Appl. Mater. Interfaces* **2017**, 9, 33989.
- [42] H. Hu, S. Moghadamzadeh, R. Azmi, Y. Li, M. Kaiser, J. C. Fischer, Q. Jin, J. Maibach, I. M. Hossain, U. W. Paetzold, B. Abdollahi Nejand, *Adv. Funct. Mater.* **2021**, 2107650.
- [43] R. N. Wenzel, *J. Phys. Colloid Chem.* **1949**, 53, 1466.
- [44] J. Yin, Y. Yuan, J. Ni, J. Guan, X. Zhou, Y. Liu, Y. Ding, H. Cai, J. Zhang, *ACS Appl. Mater. Interfaces* **2020**, 12, 48861.
- [45] Q. Lou, Y. Han, C. Liu, K. Zheng, J. Zhang, X. Chen, Q. Du, C. Chen, Z. Ge, *Adv. Energy Mater.* **2021**, 11, 2101416.
- [46] A. K. Harit, E. D. Jung, J. M. Ha, J. H. Park, A. Tripathi, Y. W. Noh, M. H. Song, H. Y. Woo, *Small* **2021**, e2104933.
- [47] G. You, L. Li, S. Wang, J. Cao, L. Yao, W. Cai, Z. Zhou, K. Li, Z. Lin, H. Zhen, Q. Ling, *Adv. Energy Mater.* **2021**, 12, 2102697.
- [48] W. Zhao, H. Li, D. Li, Z. Liu, D. Wang, S. Liu, *J. Power Sources* **2019**, 427, 223.
- [49] Y. Zhong, G. Liu, Y. Su, W. Sheng, L. Gong, J. Zhang, L. Tan, Y. Chen, *Angew. Chem., Int. Ed.* **2021**, 60, 2.
- [50] Z. Xing, S. Lin, X. Meng, T. Hu, D. Li, B. Fan, Y. Cui, F. Li, X. Hu, Y. Chen, *Adv. Funct. Mater.* **2021**, 31, 2107726.